Master's Thesis

Flexible/functional porous ceramic membranes for high-performance battery separators

Jeong-hoon Kim

Department of Energy Engineering
(Battery Science and Technology)

Graduate School of UNIST

2015

Flexible/functional porous ceramic membranes for high-performance battery separators

Jeong-Hoon Kim

Department of Energy Engineering
(Battery Science and Technology)

Graduate School of UNIST

Flexible/functional porous ceramic membranes for high-performance battery separators

A thesis/dissertation
submitted to the Graduate School of UNIST
in partial fulfillment of the
requirements for the degree of
Master of Science

Jeong-Hoon Kim

6. 18. 2015 Month/Day/Year of submission

Approved by

Advisor

Sang-Young Lee

Flexible/functional porous ceramic membranes for high-performance battery separators

Jeong-Hoon Kim

This certifies that the thesis/dissertation of Jeong-Hoon Kim is approved.

6. 18. 2015 Month/Day/Year of submission

signature

Advisor: Sang-Young Lee

signature

Soojin Park

signature

Youngsik Kim

Contents

Abstract

There is no doubt that rechargeable lithium-ion batteries occupy predominant position as a competent power source in a wide variety of industry fields including portable electronics, electric vehicles (EVs) and grid-scale energy storage systems (ESSs). For example, spinel lithium manganese oxide ($LiMn_2O_4$, LMO) materials, which are widely used in large-scale batteries for applications in EVs and ESSs, are struggling with dissolution of Mn^{2+} ions at elevated temperatures. The Mn^{2+} dissolution-triggered disruption/contamination of electrodes are known to provoke serious capacity fading during charge/discharge cycling.

As a ceramic-driven material/architecture strategy to develop an ultimate battery separator far beyond traditional polymeric separators, we have demonstrated flexible/functional porous ceramic membranes (referred to as "2F ceramic separators") with chemical traps for chelating heavy metal ions (here, Mn^{2+}). The 2F ceramic separator, which was comprised of the densely-packed F-silica particles spatially besieged by the PVP/PAN nanofiber skeleton, was fabricated using the simultaneous electrospraying/electrospinning process. The superlattice crystals-mimic structural uniqueness of the close-packed ceramic particles, in combination with the well-designed electrospun nanofiber skeleton, provided remarkable advances in the thermal/dimensional tolerance, mechanical flexibility and other separator properties. Furthermore, both the F-silica particles and PVP/PAN nanofibers possessed the Mn^{2+}-chelating ability, which served as chemical traps for Mn^{2+} ions during their passage through the liquid electrolyte-filled interstitial voids of the 2F ceramic separator. As a consequence, the 2F ceramic separator enabled unprecedented improvements in the high-performance lithium-ion batteries.

The 2F ceramic separator will hold a great deal of promise as a chemically-active separator for high-performance batteries that are eager to adopt high-energy (but, struggling with metal dissolution) electrode materials and also open a new ceramic opportunity for next-generation multifunctional membranes that are in strong pursuit of selectivity removing heavy metal ions.

List of Figures

Figure 10. (a) A SEM image of electrospun PVP nanofiber mat. (b) A photograph showing the structural disruption of electrospun PVP nanofiber mat after being immersed in liquid electrolyte (1M $LiPF_6$ in EC/DEC = 1/1 (v/v)).

Figure 11. (a) A SEM image (surface view) showing the dimensional stability of electrospun PVP/PAN nanofiber mat after being immersed in liquid electrolyte (1M $LiPF_6$ in EC/DEC = 1/1 (v/v)). (b) Amount of Mn^{2+} ions captured by PVP/PAN film (vs. PAN film).

Figure 12. Fabrication and characterization of 2F ceramic separator: (a) a SEM image of F-silica particles (insets show chemical structure of F-silica particles and physical appearance of F-silica particle solution, respectively); (b) a SEM image of electrospun PVP/PAN nanofiber mat (an inset shows chemical structure of PVP and PAN); (c) a SEM image (an inset = cross-sectional view); (d) photographs and a SEM image showing structural tolerance after being subjected to extreme deformation (here, crumpling) test. Comparison between 2F ceramic separator and PE separator; (e) amount of Mn^{2+} ions captured by the separators (estimated from ICP-MS analysis); (f) high-temperature (60 ^{o}C) cycling performance.

Figure 13. A TGA profile used for estimating the composition ratio of 2F ceramic separator. As a reference sample, TGA profiles of electrospun PVP/PAN nanofiber mat and F-silica were also provided.

Figure 14. Comparision in basic membrane properties between 2F ceramic separator and PE separator: (a) electrochemical stability window measured by linear sweep voltammetry; (b) thermal shrinkage after exposure to 150 ^{o}C/0.5 h; (c) electrolyte wettability (determined by electrolyte-immersion height).

Figure 15. Comparison in cycling performance between 2F ceramic separator and PE separator: (a) charge/discharge profiles as a function of cycle number; (b) change in AC impedance spectra before/after 100 cycles.

Figure 16. (a)-(c) Structural analysis of LMO cathode and Li metal anode after 100 cycles at 60 ^{o}C: (a) metallic Mn deposited on lithium metal anode (from ICP-MS analysis); (b) a SEM image of LMO cathode surface assembled with 2F ceramic separator, wherein an inset shows LMO cathode surface assembled with PE separator; (c) XPS F 1s spectra of LMO surface. (d)-(f) Structural analysis of 2F ceramic separator 100 cycles at 60 ^{o}C: (d) a SEM image; (e) FT-IR spectra showing the change in characteristic peaks of thiol (2580 cm^{-1}, F-silica) and C=O/C-N groups (1661 cm^{-1}/1285 cm^{-1}, PAN/PVP nanofiber skeleton); (f) intensity change of XPS S 2p spectra.

Figure 17. A SEM image of PE separator after 100 cycles at 60 ºC.

Figure 18. Structural analysis of 2F ceramic separator after 100 cycles at 60 ºC: (a) EDS spectra (focusing on Mn element); (b) XPS F 1s spectra.

Figure 19. A conceptual illustration depicting advantageous effect of 2F ceramic separator on high-temperature cycling performance. A considerable amount of dissolved Mn^{2+} ions are captured by the 2F ceramic separator in the form of Mn(II) chelate complexes, eventually suppressing the Mn^{2+} ions-triggered negative influence on the electrochemical performance of electrodes.

List of Table

CHAPTER I. INTRODUCTION

1.1. Operating principle of lithium-ion batteries

The endless pursuit of rechargeable lithium-ion batteries, which are demanded a wide variety of industry fields as a commercial power source regarding portable electronics, electric vehicles (EVs) and grid-scale energy storage systems (ESSs). Also, the lithium-ion batteries are essentially required reliable electrochemical properties and reinforced safety tolerance, because they are having with serious problems about safety failures of cells and the performance deterioration. A conventional lithium-ion batteries are made up of four core components, i.e., two electrodes of the cathode (positive electrode) and anode (negative electrode), electrolyte and separator (Figure 1). During charging reaction of the battery, lithium ions transfer through electrolyte-filled porous channels of separator from cathode to anode and the electrons pass through the external circuit at the same time (Equation 1). Also, when the battery is discharged, the reaction is a reverse reaction of a previous process (Equation 2).[1, 2] For example, using conventional lithium-ion batteries, the $LiCoO_2$ cathodes and graphite anodes have been explained below equations

$$\text{Cathode side: } LiCoO_2 \leftrightarrows Li_{1-x}CoO_2 + xLi^+ + xe^- \quad (1)$$

$$\text{Anode side: } xLi^+ + xe^- + xC_6 \leftrightarrows xLiC_6 \quad (2)$$

$$\text{Total reaction: } LiCoO_2 + xC_6 \leftrightarrows Li_{1-x}CoO_2 + xLiC_6 \quad (3)$$

(→: Charge reaction, ←: Discharge reaction)

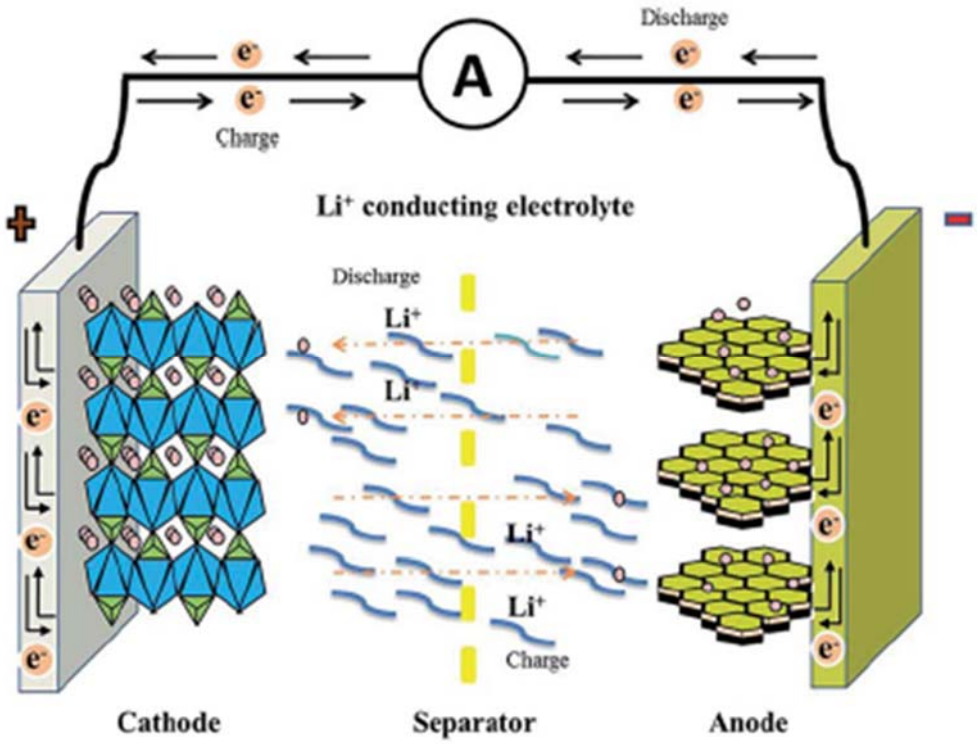

Figure 1. A schematic diagram of representative lithium-ion batteries: Cathode, Anode, Electrolyte and Separator.

The separator is consisted a porous structure and is located between the cathode and anode. In a lithium-ion batteries, the separator is one of a core components, it is able to ionic transport phenomena as the electrolyte-filled porous channels. Also, the separator has to take a role of an electronic insulators for preventing internal short-circuit. Besides, properties of the separator are influenced in the battery system, considering cycle ability, energy density, power density, and safety. As a result, it should have properties such as well-defined porous structure, ultimate thermal stability, and the better electrolyte wettability. In this regard, the characteristics of the separator should be concerned for a wide range of use in lithium-ion batteries. The lithium-ion batteries separators are divided into two classes such as polyolefin separators and nonwoven mat separators. Firstly, the polyolefin separators are fabricated from polyethylene (PE), polypropylene (PP). Also, they are combined PE with PP such as PE/PP and PP/PE/PP.[1, 2] In addition, other polymers have been used for the polyolefin separators. Despite such commercial popularity, the polyolefin separators remain a formidable obstacle to further advancement of the batteries, due to the intrinsic limitations arising from incomplete porous structure and poor thermal/mechanical stability. Secondly, the nonwoven mat separators are consisted of fibrous structures and the fibers are bonded together by chemical or thermal bonding. The nonwoven mats are traditionally made various ways such as dry and wet processes. In general, they are often used as separators for several types of batteries: alkaline, Ni-Cd and lead acid batteries. There are the materials for preparing nonwoven mats, like polyethylene (PE), polypropylene (PP), polyamide (PA), poly(tetrafluoroethylene) (PTFE), polyvinylidine fluoride (PVdF), and poly(vinyl chloride) (PVC).[1, 2] However, it is not good for them to use the lithium-ion batteries because of the physical properties regarding unsuitable pore size, large fiber diameter and difficulty in making thin. To improve the drawbacks, the electrospinning method (Figure 2) has been used to fabricate highly porous structure nonwoven mat separators that are suitable for lithium-ion batteries. The electrospinning method has a reputation for a simple and efficient technique as fabricating nonwoven mat separators. Also, it has many advantages that can be controlled the porous structure of nonwoven mat separators such as high porosity, small pore size, interconnected open pore structure, high permeability, and large surface area.[2]

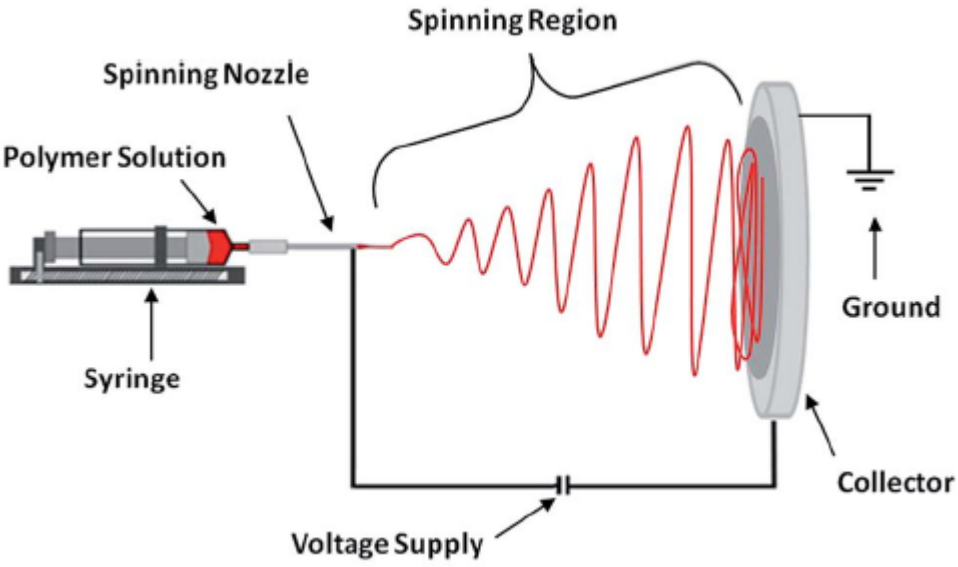

Figure 2. A schematic diagram of representative electrospinning method.

1.2. General requirements for battery separators

During the battery process, separators have to stable to strong oxidizing and reducing conditions because they should overcome the unwanted byproduct of the electrolyte at elevated temperatures. As a result, they are required a wide variety of properties. They are listed in Table 1.[1-3]

The electrolyte wettability of separators is required, it causes ion transport during the battery operation. Good wettability is able to achieve low internal resistance and high ionic conductivity. Also, separators have to absorb lots of liquid electrolyte, it should keep porous structures of the separators. Besides, when the battery are assembled, the electrolyte filling time shortens as soon as possible. Since the time is affect the battery's life cycle. There are the factors of filling speed such as the materials, porosity and pore size.

The mechanical properties of separators are usually required for the tensile strength and puncture strength. During battery assembly, they should have the surmountable tension regarding the winding operation. Separators must be have the remarkable puncture strength because, it helps to suppress internal short circuit that is caused by lithium dendrite growth or particles from moving the electrodes.

Although separator in the battery have been using 20-50μm in thickness, separators are required in the range of 20-25μm. Because thin separators could have advantages as lower inter resistance, high energy, and power densities. On the other hand, thicker separators could also have various characteristics, like easy handling, outstanding safety in the battery. Since they give higher mechanical strength. For these reasons, the thickness of separators should be optimized for a suitable using in a commercial battery.

The thermal shrinkage of separators is demanded generally less than 5% after 60min at 90oC. It is need to suppress the battery operation from overheating or electrical shorting. Also, it is a desirable safety function of separators. Besides, if the battery is operate in the thermal runaway, separators should close the pores and block ionic flows. Nowadays, the thermal properties of separators is required at 130^{o}C, so needing the ultimate thermal polymers.

Finally, the items regarding the pore of separators is more important factor. The separators are consisted of small mean pore size for blocking particles such as active materials of the electrodes and conducting additives. The pore size distributions should also be uniform in separators because of avoiding the non-uniform current densities. The non-uniform current between the electrode and separator cause the formation of dendrite growth. In addition, the tortuous structure of the pore help to control dendritic lithium. Currently, pores of separators are required submicron pore size (less than 1um).

Parameter	Requirement
Chemical and electrochemical stabilities	Stable for a long period of time
Wettability	Wet out quickly and completely
Mechanical property	>1000 kg cm^{-1} (98.06 MPa)
Thickness	20–25 μm
Pore size	<1 μm
Porosity	40–60%
Permeability (Gurley)	<0.025 s μm^{-1}
Dimensional stability	No curl up and lay flat
Thermal stability	<5% shrinkage after 60 min at 90 °C
Shutdown	Effectively shut down the battery at elevated temperatures

Table 1. The items of considering commercial separators in lithium ion batteries.

CHAPTER II. FLEXIBLE/FUNCTIONAL POROUS CERAMIC MEMBRANES FOR HIGH-PERFORMANCE BATTERY SEPARATORS

2.1. Introduction

There is no doubt that rechargeable lithium-ion batteries occupy predominant position as a competent power source in a wide vareity of industry fields including portable electronics, electric vehicles (EVs) and grid-scale energy storage systems (ESSs).[4-7] To boost continuous progress and applicability extension of the batteries, reliable/sustainable electrochemical properties and reinforced safety tolerance are essentially required.[8, 9] Taking into account the fact that electrochemical performance of the batteries is basically determined by electron/ion transport phenomena, particular attention should be paid to battery separators as well as electrodes/electrolytes, because i) all ions engaged in Faradaic reaction of batteries should pass through electrolyte-filled porous channels of battery separators; ii) internal short-circuit failure between electrodes (that is considered as a major cause to trigger cell fire or explosion) is eventually prevented by battery separators.[1, 2, 10]

Currently commercially-available separator membranes for lithium-ion batteries are porous polyolefin ones. Despite such commercial popularity, the polyolefin separators remain a formidable obstacle to further advancement of the batteries, due to the intrinsic limitaions arising from incomplete porous structure and poor thermal/mechanical stability.[2] To overcome these problems, a number of separator strategies have been suggested,[11-14] including nanopartcles-coated separators, nonwoven separators and electrospun fiber separators. Moving back to the basic roles of battery separators (as ion-conducting channels and also electronic insulators between electrodes), ceramic membranes with well-defined porous structure could be recommended as a promising solution to address the aforementioned challenges of polymer-based separators, because they exhibit ultimate thermal stability/dimensional rigidity that could be effective in preventing internal short-circuit failure. Typical porous ceramic membranes,[15, 16] however, are manufactured through high-pressure/high-tempreature sintering of ceramic particles. As a result, they tend to be easily fragile and thus fail to withstand structural integrity upon mechanical deformation. In addition, thickness reduction is another challenging issue in the development of ceramic membranes. For these reasons, no meaningful results have been reported with ceramic membranes for battery separator applications.

Among numerous architecutral innovations of advanced materials, superlattice crystals, which are characterized with highly-ordered/close-packed particle arrays, have been extensively investigated as a compelling building template in a wide variety of application fields such as photonic crystals, catalysts, electrodes and sensors.[17-19] From the viewpoint of battery separator requirements, the close-packed particle arrays of superlattice crystals are expected to offer exceptional benefits for the thermal stability, dimensional rigidity and, more notably, porous structure (i.e., interstitial voids formed between the particles), although they are mechanically fragile upon external deformation stress.

Considering again the key role[1, 2, 10] of battery separators as ion-conducting channels between electrodes, functional separators bearing chemical traps (that can capture unwanted heavy metal ions dissolved in liquid electrolyte) are expected to provide beneficial effects on cell performance. For example, spinel lithium manganese oxide ($LiMn_2O_4$, LMO) materials,[20, 21] which are widely used in large-scale batteries for applications in EVs and ESSs, are struggling with dissolution of Mn^{2+} ions at eleveated temperatures. The Mn^{2+} dissolution-triggered disruption/contamination of electrodes are known to provoke serious capacity fading during charge/discharge cycling. Most of previous studies on this issue have been devoted to synthesis/engineering of cathode materials, functional binders and electrolytes.[22-25] Unfortunately, very few works,[26, 27] which were focused on the surface modification of polyethylene (PE) separators, were reported with battery separators.

Here, inspired by the abovementioned structural novelty/potential benefits of ceramic membranes/superlattice crystals and also spurred by the urgent demand for chemical traps of heavy metal ions, we demonstrate a new class of ultimate battery separator based on flexible/functional porous ceramic membranes (referred to as "2F ceramic separators") for high-performance lithium-ion batteries. The 2F ceramic separators are comprised of densely-packed ceramic particles spatially besieged by electrospun nanofiber skeleton. Both the ceramic particles and nanofibers are rationally designed and synthesized to provide well-developed porous structure and also chemical functionality (as a new concept of chemical trap for chelating unwanted heavy metal ions dissolved in electrolytes). The compactly-packed ceramic particles in the 2F separators, similar to the superlattice crystals, offer exceptional thermal stability/dimensional rigidity and allow the formation of three-dimensionally (3D)-reticulated interstitial voids (that will be filled with liquid electrolyte). The electrospun nanofibers are introduced as a reinforcing skeleton to hold the compactly-packed ceramic particles, thereby contributing to mechanical flexibility and toughness without the aid of typical polymeric binders. Owing to such material/structural uniqueness, the 2F separators are expected to enable unprecedented improvements in membrane properties and also cell performance far beyond those accessible with conventional polymeric battery separators.

2.2. Experimental

2.2.1. Synthesis of thiol-functionalized silica (F-silica) particles and PVP/PAN blends

As a core component of the 2F ceramic separators, thiol (-SH)-functionalized silica (F-silica) particles were synthesized by sol-gel process using 3-mercaptopropyl trimethoxysilane (MPTMS) as a precursor. 5 g of MPTMS was mixed with 500 g of water until the solution became transparent. Subsequently, 0.25 ml of ammonium hydroxide was added into the transparent solution. The mixture solution went through sol-gel reaction at 40 ^{o}C for 17 h. After the precipitation followed by washing of non-reactive materials, the F-silica particles were obtained. To prepare another key component of the 2F ceramic separators, PVP/PAN blends, PAN (molecular weight = 150,000 g mol^{-1}) and PVP (molecular weight = 1,300,000 g mol^{-1}) were dissolved in dimethylacetamide (DMAc) at 70 ^{o}C for 12 h, where the total polymer concentration was 20 wt.% and the relative composition ratio of PVP/PAN was 50/50 (w/w).

2.2.2. Structural design and fabrication of 2F ceramic separator

To fabricate the 2F ceramic separator, we exploited the simultaneous electrospraying (for densely-packed ceramic particles)/electrospinning (for nanofiber skeletons) technique followed by roll pressing. For a model ceramic separator comprising the densely-packed Al_2O_3 particles and PVdF nanofiber skeletons, the Al_2O_3 colloidal solution (5 wt.% Al_2O_3 in acetone/n-butanol (= 7/3 v/v)) and PVdF solution (25 wt.% PVdF in dimethylacetamide/acetone (= 7/3 v/v)) were respectively prepared and then sbujected to simulatneous electropraying/electrospinning through two different nozzles at room temperature. The detailed experimental conditions were 10.0 kV with a feed rate of 5 μL min^{-1} (for electrospinning) and 17.5 kV with a feed rate of 70 μL min^{-1} (for electrospinning). The resulting Al_2O_3/PVdF mixture mat was collected on a stainless steel plate positioned at a distance of 12 cm from the nozzles. After being roll-pressed at room temperature, a self-standing and flexible ceramic separator (thickness ~ 30 μm) was produced. The 2F ceramic separator (thickness ~ 30 μm), which consisted of F-silica particles and PVP/PAN blend skeleton, was fabricated by the simultaneous electrospraying (14.0 kV with a feed rate of 50 μL min^{-1})/electrospinning (8.0 kV with a feed rate of 3.5 μL min^{-1}) process used for the model ceramic separator. A commercial PE separator (thickness = 20 μm, Tonen) was chosen as a control sample.

2.2.3. Structural/physicochemical characterization of 2F ceramic separator

The surface and cross-sectional porous morphology of the 2F ceramic separator was analyzed with FE-SEM (S-4800, Hitachi) and EDS (JSM 6400, JEOL). The electrolyte wettability of the separator was estimated by measuring the electrolyte immersion-height. The thermal shrinkage of the separator was examined by measuring their area-based dimensional change after exposure to 150 ^{o}C/0.5

h. The composition ratio of the separator was determined from the TGA measurement (SDT Q600, TA Instruments) at a heating rate of 10 ^{o}C min^{-1} under air atmosphere. The chemical structure of the F-silica was identified using FT-IR spectrometer (670-IR, Agilent). The Mn^{2+}-chelating ability of the separator and its components was quantitatively estimated by measuring the amount of the captured Mn^{2+} ions using ICP-MS analysis (ELAN DRC-II, Perkin Elmer), wherein the samples were immersed in the manganese perchlorate solution[22] (10 mM $Mn(ClO_4)_2$-containing 1.3 M $LiPF_6$ in EC/PC = 1/1 v/v) for 2 h at room temperature. For the PE separator, in order to improve its poor electrolyte wettability, the surface treatment (specifically, soaking the separator into 1N H_2SO_4 solution for 2 h at 90 ^{o}C) was applied before being immersed in the manganese perchlorate solution. The structural change of electrode surface and seaparators after the charge/discharge cycling test was analyzed using XPS (ThermoFisher) with focused monochromatized Al Kα radiation.

2.2.4. Electrochemical properties of 2F ceramic separator and its application to lithium-ion batteries

The electrochemical stability window of the 2F ceramic separator was investigated using a linear sweep voltammetry experiment performed on a working electrode of stainless-steel and a counter/reference electrode of lithium-metal at a scan rate of 1.0 mV s^{-1}. The OCV drop of the fully charged cell (at a current density of 0.2 C) was monitored as a function of elapsed time. The ionic conductivity of the separator was examined by an AC impedance analysis (VSP classic, Bio-Logic) over a frequency range of 10^{-2} - 10^{6} Hz. A pouch-type cell (width x length = 30 x 40 mm/mm) was assembled by sandwiching a separator between LMO cathode (LMO/carbon black/PVdF = 92/3/5 w/w/w, areal mass loading = 17 mg cm^{-2}) and Li metal anode, and then activated by being filled with the liquid electrolyte (1 M $LiPF_6$ in EC/DEC = 1/1 v/v). The cell performance was investigated using a cycle tester (PNE Solution) at 25 and 60 ^{o}C under various charge/discharge conditions.

2.3. Results and discussion

2.3.1. A preliminary step for 2F ceramic separator: Fabrication of a model ceramic separator comprising Al_2O_3 particles and PVdF fibers

To fabricate the 2F ceramic separators, we exploited the simultaneous electrospraying (for densely-packed ceramic particles)/electrospinning (for nanofiber skeletons) technique followed by roll pressing, instead of classical sintering processes that require harsh operating conditions of high-temperature/high-pressure. A schematic illustration depicting the manufacturing procedure of the 2F ceramic separators was presented in Figure 3a. The basic concept of the combined electrospinning/electrospraying process was already reported for the preparation of nanocomposite nonwovens.[28, 29] However, in contrast to the 2F ceramic separators presented herein (i.e., characterized with densely-packed ceramic particles besieged by electrospun nanofiber skeleton), the previous works were just limited to the simple modification of polymer fabrics with ceramic powders.

As a preliminary step for the development of 2F ceramic separators, a model ceramic separator comprising Al_2O_3 particles and polyvinylidene fluoride (PVdF), both of which were not chemically active, was fabricated with the aim of exploring feasibility of the simultaneous electrospraying/electrospinning-driven manufacturing process and also investigating basic properties of the ceramic separator. The Al_2O_3 colloidal solution (5 wt.% Al_2O_3 in acetone/n-butanol (= 7/3 v/v)) and PVdF solution (25 wt.% PVdF in dimethylacetamide/acetone (= 7/3 v/v)) were respectively prepared and then subjected to simultaneous electrospraying/electrospinning through two different nozzles. After being roll-pressed at room temperature, a self-standing and flexible ceramic separator (thickness ~ 30 μm) was produced (Figure 3b). From the thermogravimetric analysis (TGA) measurement (Figure 4), the composition ratio of the ceramic separator was found to be Al_2O_3/PVdF = 65/35 (w/w). The SEM images (Figure 3c) show that the ceramic separator is composed of electrosprayed, densely-packed Al_2O_3 particles surrounded by electrospun PVdF nanofiber skeleton. Porous structure (that will be filled with liquid electrolyte) of separators is known to play an important role as an ion-conducting channel between electrodes. The ceramic separator exhibits the 3D-reticulated/highly-developed interstitial voids formed between the Al_2O_3 particles (Figure 3c), eventually contributing to the superiority in ion transport (σ(ionic conductivity) = 1.6 mS cm^{-1} for ceramic separator vs. 0.9 mS cm^{-1} for a commercial PE separator (Figure 5) chosen as a control sample).

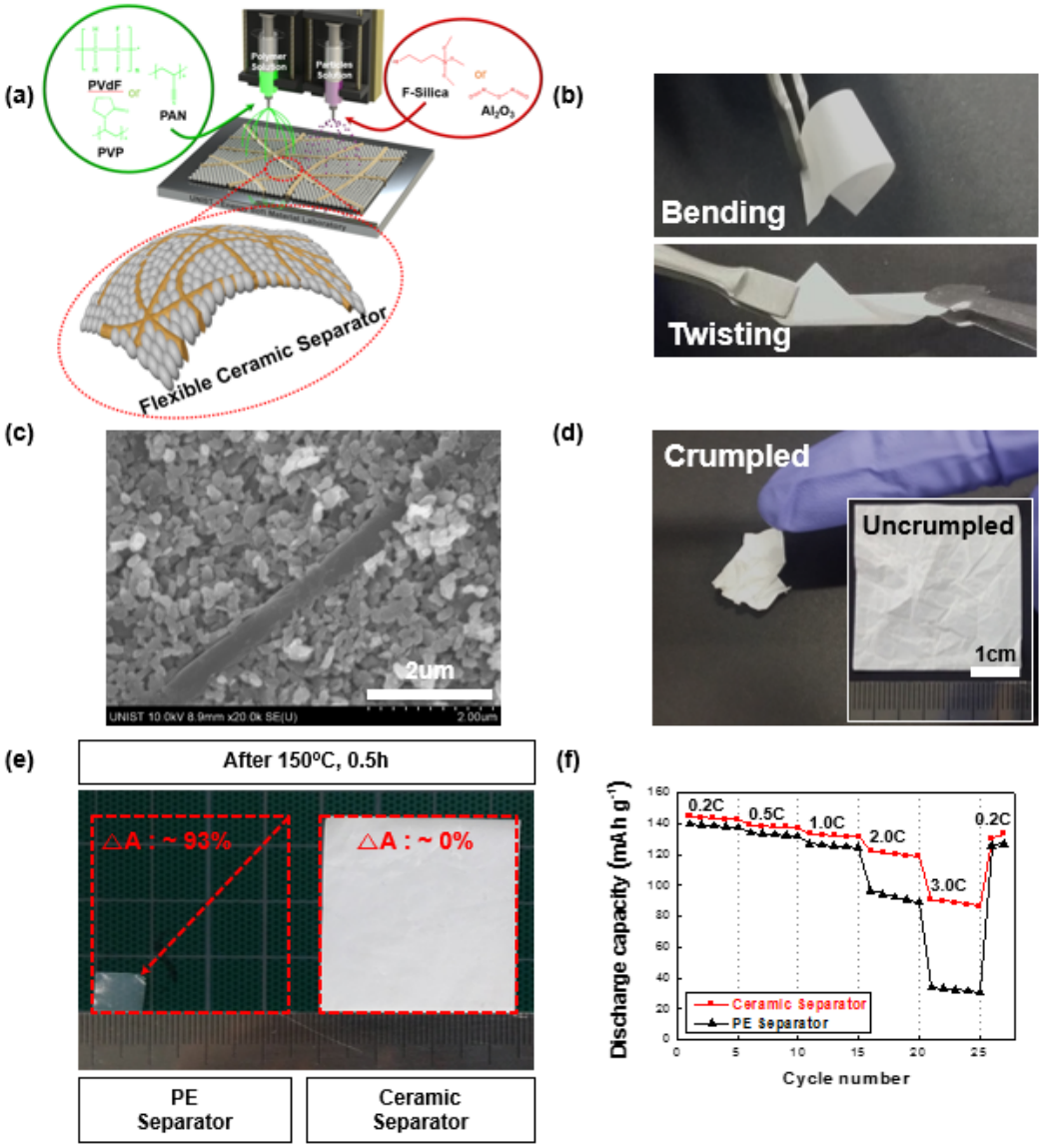

Figure 3. (a) A schematic illustration depicting the manufacturing procedure of 2F ceramic separators via simultaneous electrospraying/electrospinning process. Characterization of model (Al_2O_3/PVdF-based) ceramic separators: (b) photographs showing the self-standing and flexible ceramic separator; (c) a SEM image (surface view); (d) photographs showing the structural tolerance upon external deformation (here, crumpling) stress, wherein an inset shows the model ceramic separator after being uncrumpled. Comparison between the model ceramic separator and PE separator; (e) thermal shrinkage after exposure to 150 °C/0.5 h; (f) discharge rate capability of cells ($LiCoO_2$ cathode ($LiCoO_2$/carbon black/PVdF = 95/2.5/2.5 (w/w/w)) and graphite anode (graphite/carbon black/SBR/CMC = 96/1/2/1 (w/w/w)).

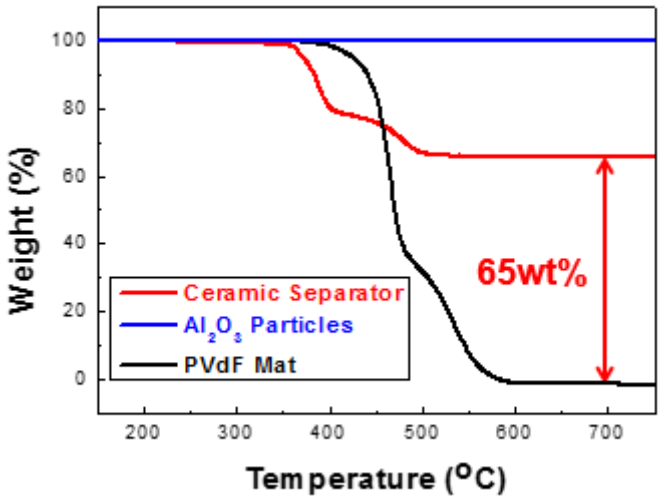

Figure 4. A TGA profile used for estimating the composition ratio of model (Al_2O_3/PVdF-based) ceramic separator. As a reference sample, a TGA profile of electrospun PVdF mat was also provided.

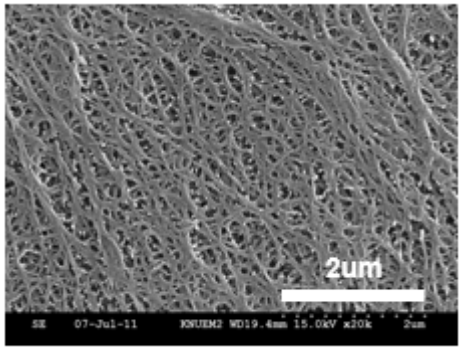

Figure 5. A SEM image (surface view) of PE separator.

To address the concern on fragility/stiffness of the ceramic separator, an extreme deformation (here, crumpling) test was performed. Even after being crumpled and subsequently uncrumpled, neither particle detachment nor mechanical disintegration of the ceramic separtor was observed (Figure 3d, Figure 6a). Such structural tolerance of the ceramic separator was further verified by measuring open circuit voltage (OCV) drop of cells as a function of elapsed time (Figure 6b). After the crumpling test, no detectable level of OCV drop was observed at the cell incorporating the ceramic separator, which appeared comparable to the OCV results of the ceramic separator (before being crumpled) and also PE separator. A primary advantage of the ceramic separator is the provision of ultimate thermal tolerance. Notably, the ceramic separator was not thermally shrunk after exposure to 150 ^{o}C/0.5 h (Figure 3e), in comparison to the PE separator (thermal shrinkage (ΔA) ~ 93 %).

The effect of the ceramic separator on the cell performance was examined, wherein $LiCoO_2$ and graphite powders were chosen as electrode active materials to explore the applicability of the ceramic separator to lithium-ion batteries. The coin cell (2032-type) assembled with $LiCoO_2$ cathode ($LiCoO_2$/carbon black/PVdF = 95/2.5/2.5 (w/w/w), areal mass loading = 19 mg cm^{-2}) and graphite anode (graphite/carbon black/styrene butadiene rubber (SBR)/carboxymethyl cellulose (CMC) = 96/1/2/1 (w/w/w), areal mass loading = 9 mg cm^{-2}) was charged at a constant current density of 0.2 C (= 0.54 mA cm^{-2}) and discharged at various current densities ranging from 0.2 to 3.0 C. The ceramic separator showed the higher discharge capacities over a wide range of discharge current densities, which became more pronounced as the discharge current density was increased (Figure 3f). The detailed charge/discharge profiles of the cells were provided in Figure 7. Such superior rate performance of the ceramic separator can be explained by its higher ionic conductivity arising from the well-developed interstitial voids filled with liquid electrolyte. These results demonstrate the structural/physicochemical excellence of the ceramic separator and also its advantageous contribution to cell performance as an alternative separator.

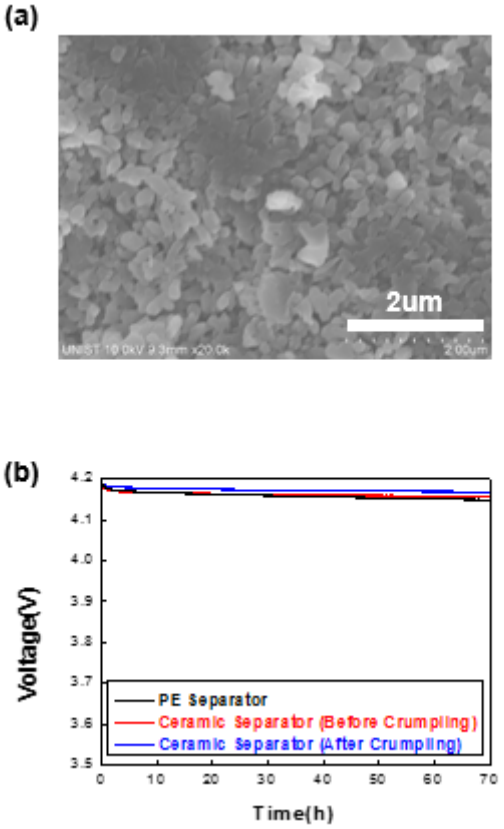

Figure 6. Structural tolerance of the model (Al_2O_3/PVdF-based) ceramic separator after being subjected to extreme deformation (here, crumpling) test: (a) A SEM image; (b) OCV drop of cells as a function of elapsed time.

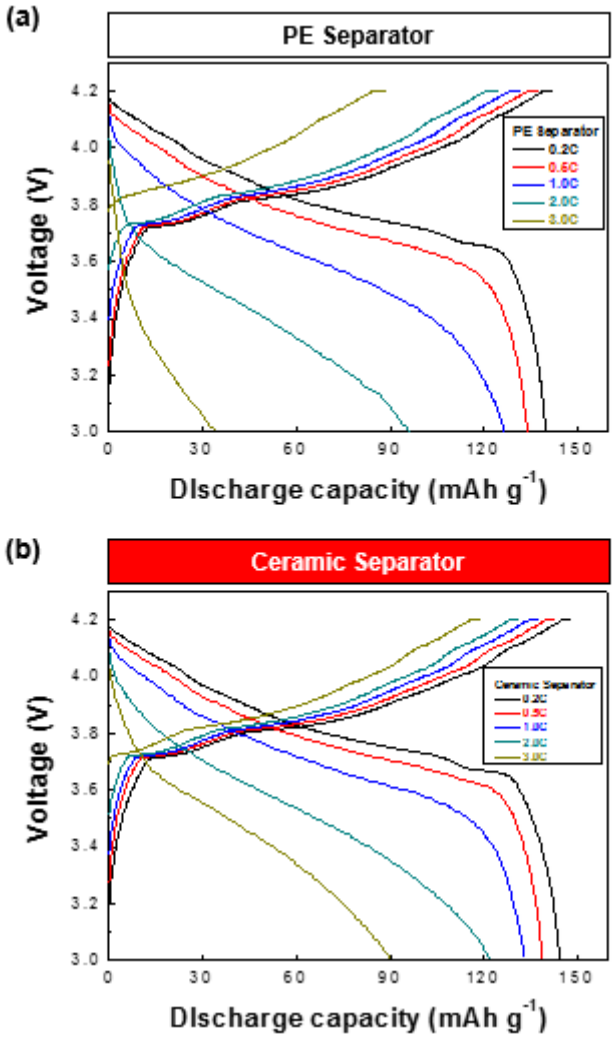

Figure 7. Comparison in charge/discharge profiles of cells as a function of discharge current density between: (a) PE separator; (b) model (Al_2O_3/PVdF-based) ceramic separator.

2.3.2. A main step for 2F ceramic separator: Fabrication and characterization of 2F ceramic separator

Based on the understanding of the model ceramic separator mentioned above, we developed the chemically-active 2F ceramic separator. As a prerequisite step, core components (i.e., functional ceramic particles and polymer nanofibers) of the 2F ceramic separator were respectively prepared, where the functionality of both core materials was designed to chelate heavy metal ions dissolved in liquid electrolytes. Here, thiol (-SH)-functionalized silica (denoted as "F-silica") particles were synthesized by sol-gel process using 3-mercaptopropyl trimethoxysilane (MPTMS) as a precursor.[30] The synthetic scheme of the F-silica was described in the experimental section (Figure 8). Thiol groups are known to effectively react with heavy metal ions through their lone pair electrons-mediated coordination bonds, eventually yielding metal-thiol complexes.[31, 32] Intriguingly, the metal-thiol complexes have been widely used to remove toxic heavy metal ions particularly in water purification systems.[33, 34]

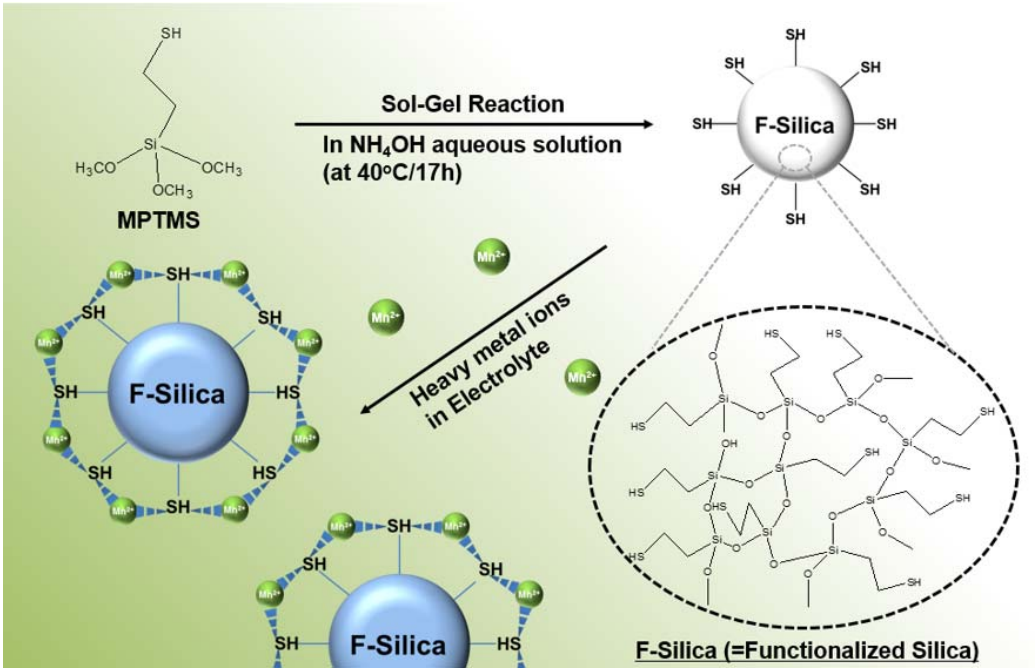

Figure 8. Schematic representation depicting the synthetic route of F-silica particles and the formation of metal ion (here, Mn^{2+})-thiol complexes.

Figure 12a shows the successful synthesis of spherical F-silica featuring well-defined particle size (~ 1 μm) and also uniform size distribution. The Fourier-transform infrared (FT-IR) spectra (Figure 9a) present characteristic peaks ascribed to the F-silica.[30, 31] Two separated peaks (1000 and 1150 cm^{-1}) indicate that symmetry of Si-O-Si bonds, which is observed in pure silica particles, is partially destroyed by the formation of Si-C bonds in the F-silica. In addition, a characteristic peak at 2580 cm^{-1} corresponding to thiol groups was observed at the F-silica. The presence of thiol groups was further confirmed by the energy dispersive X-ray spectroscopy (EDS) analysis of sulfur (S) element (Figure 9b). Metal ion chelating ability of the F-silica particles was quantitatively estimated by measuring the amount of Mn^{2+} ions trapped on F-silica particles, wherein the F-silica particles were soaked in manganese percholate ($Mn(ClO_4)_2$) electrolyte solution[22] (10 mM $Mn(ClO_4)_2$-containing 1.3 M $LiPF_6$ in EC/PC = 1/1 v/v) prior to the measurement. The inductively coupled plasma mass spectrometry (ICP-MS) analysis exhibits that the amount of Mn^{2+} ions captured by the F-silica particles is almost 10 times larger than that of Al_2O_3 particles chosen as a control sample (Figure 9c). This result demonstrates that the F-silica particles effectively chelate Mn^{2+} ions dissolved in the electrolyte solution.

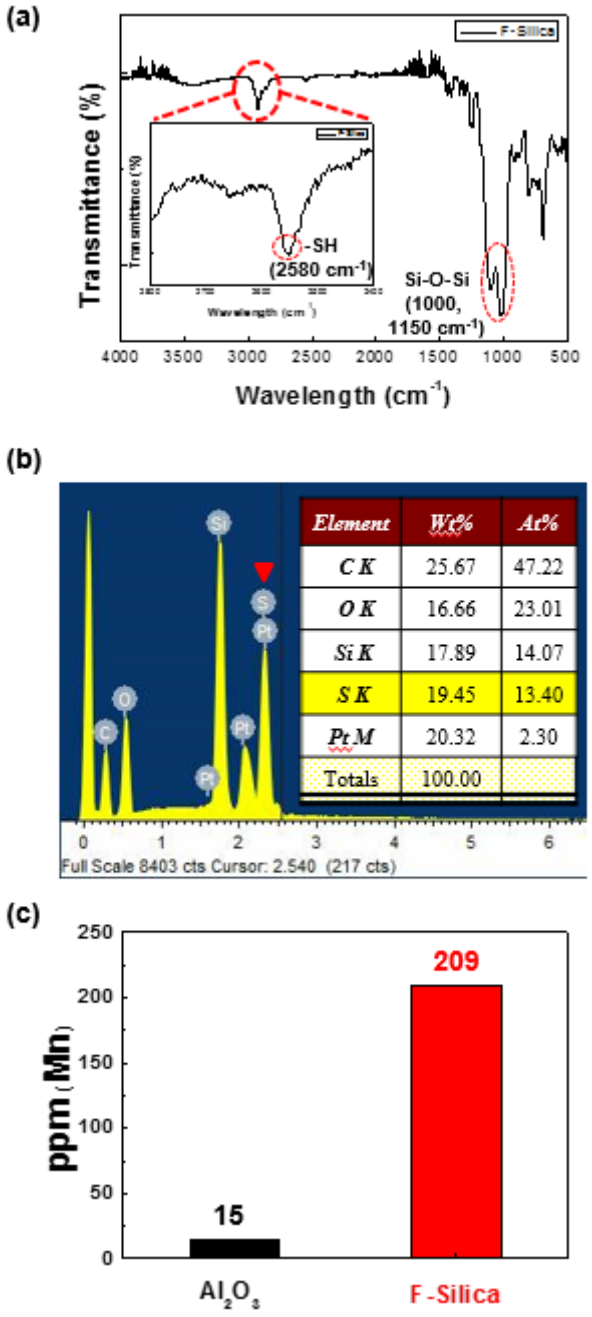

Figure 9. Structural characterization of F-silica: (a) FT-IR spectra; (b) EDS spectra (focusing on S element); (c) amount of Mn^{2+} ions captured by F-silica particles (vs. Al_2O_3 particles).

As a chemically-active nanofiber skeleton, a polymer blend based on polyacrylonitrile (PAN) and polyvinylpyrrolidone (PVP) was suggested. The PVP was chosen as a metal-ion chelating agent owing to the presence of pyrrolidone groups that can capture heavy metal ions.[35] An electrospun PVP nanofiber mat was fabricated (Figure 10a), however, easily lost its dimensional stability upon exposure to liquid electrolyte such as 1M $LiPF_6$ in EC (ethylene carbonate)/DEC (diethyl carbonate) = 1/1 (v/v) (Figure 10b). To resolve this chemical instability of PVP, a polymer blend concept was introduced, where PAN that is chemically stable in the liquid electrolyte was mixed with PVP. The PVP/PAN (= 1/1 (w/w)) blend was electrospun, leading to the generation of PVP/PAN nanofiber mat. A number of the nanofibers were piled up with being randomly intercrossed (Figure 12b). In contrast to the pristine PVP nanofiber mat, the PVP/PAN nanofiber mat can maintain its dimensional stability after being immersed in the same liquid electrolyte (Figure 11a). To elucidate the chelating ability of the PVP/PAN nanofiber mat, the same Mn-trapping test used for the F-silica particles was conducted. Here, to avoid unwanted misunderstanding arising from porous structure of the nanofiber mats, the PVP/PAN film (not PVP/PAN nanofiber mat) was prepared as a model sample and its Mn^{2+} ion chelating ability was examined. As expected, substantial improvement in the chelating ability was observed at the PVP/PAN film, which was approximately 40 times larger than that of the PAN film chosen as a control sample (Figure 11b).

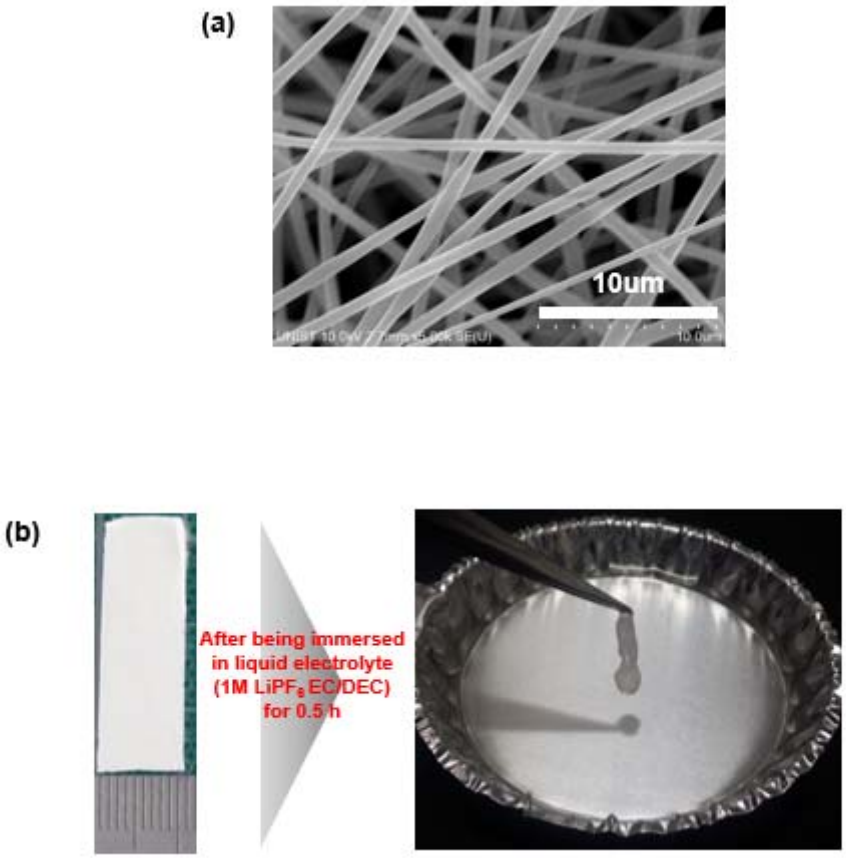

Figure 10. (a) A SEM image of electrospun PVP nanofiber mat. (b) A photograph showing the structural disruption of electrospun PVP nanofiber mat after being immersed in liquid electrolyte (1M LiPF6 in EC/DEC = 1/1 (v/v)).

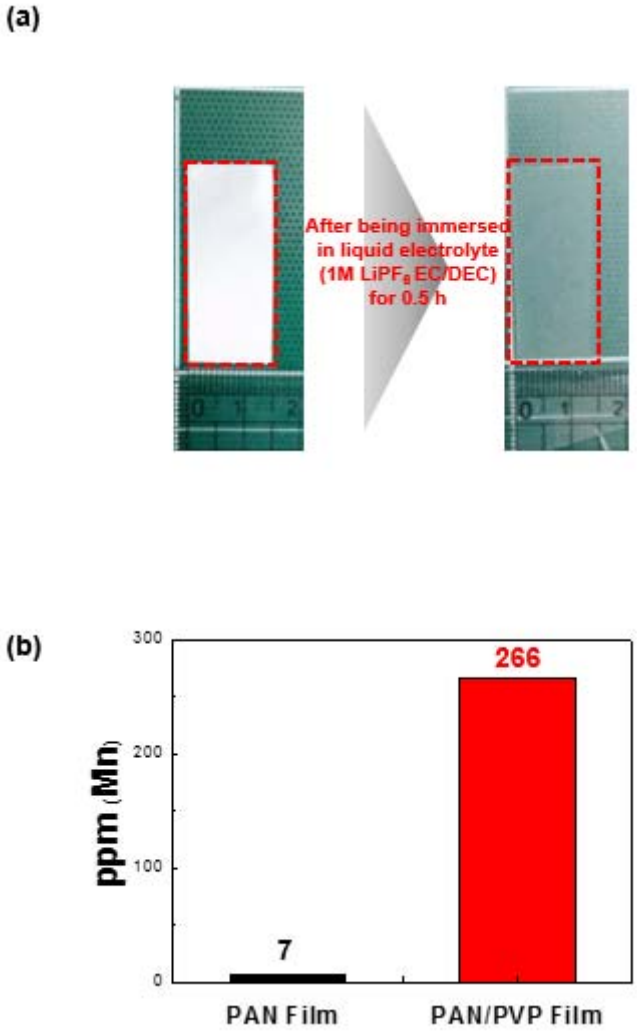

Figure 11. (a) A SEM image (surface view) showing the dimensional stability of electrospun PVP/PAN nanofiber mat after being immersed in liquid electrolyte (1M $LiPF_6$ in EC/DEC = 1/1 (v/v)). (b) Amount of Mn^{2+} ions captured by PVP/PAN film (vs. PAN film).

After the preparation of the chemically-active core components (i.e., F-silica particles and PVP/PAN blends), we fabricated the 2F ceramic separator (thickness ~ 30 μm) using the simultaneous electrospraying/electrospinning process adopted for the Al_2O_3/PVdF-based model ceramic separator. The details on the fabrication procedure of the 2F ceramic separator were described in the experimental section. The composition ratio of the 2F ceramic separator was observed to be F-silica/(PVP/PAN) = 54/46 (w/w), from the TGA measurement (Figure 13).

The structural uniqueness and membrane properties of the 2F ceramic separators were investigated. Figure 12c shows that the 2F ceramic separator comprises the electrosprayed F-silica particles spatially besieged by the PVP/PAN nanofiber skeleton. The densely-packed F-silica particles allow the formation of 3D-reticulated interstitial voids which act as ion-conducting channels, thus providing good ionic conductivity (1.4 mS cm^{-1} for 2F ceramic separator vs. 0.9 mS cm^{-1} for PE separator). The 2F ceramic separator maintained its structural stability even after being crumpled and uncrumpled (Figure 12d). The electrochemical stability of the ceramic separator was examined using linear sweep voltammetry (LSV). No appreciable decomposition of the ceramic separator was observed up to 4.5 V (vs. Li/Li^+), which appears comparable to that of the PE separator (Figure 14a). The ultimate thermal tolerance was also observed at the 2F ceramic separator, i.e., no thermal shrinkage at 150 °C/0.5 h (Figure 14b). The 2F ceramic separator, owing to polar characteristics of its components and well-developed porous structure, showed the higher electrolyte-immersion height than the PE separator (Figure 14c), demonstrating the better electrolyte wettability. In addition to such excellence in the membrane properties, another salient feature of the 2F ceramic separaotor is the chelating ability of Mn^{2+} ions. Figure 12e shows that, owing to the presence of the chemically-active F-silica particles and also PVP/PAN nanofiber skeleton, the 2F ceramic separator enabled the remarkable improvement in the Mn^{2+} chelation (the amount of captured Mn^{2+} ions: 202 ppm for 2F ceramic separator vs. 14 ppm for PE separator).

A pouch-type cell (width x length = 30 x 40 mm/mm) assembled with LMO cathode (LMO/carbon black/PVdF = 92/3/5 (w/w/w), areal mass loading = 17 mg cm^{-2}) and Li metal anode was cycled between 3.0 and 4.3 V at a charge/discharge current density of 1.0 C (= 1.86 mA cm^{-2})/1.0 C. The cell incorporating the 2F ceramic separator showed the stable high-temperature (60 °C) charge/discharge profiles up to 100 cycles (Figure 15a). By comparison, the cell containing the PE separator presented a sharp decay in capacity and large cell polarization particularly after 100 cycles. The capacity retention after 100 cycles was approximately 94 % for the 2F ceramic separator and 0 % for the PE separator (Figure 12f). Such better capacity retention was confirmed by analyzing the variation in the AC impedance spectra of the cells before/after 100 cycles (Figure 15b). The cell with the 2F ceramic separtor remarkably suppressed the growth of the cell impedance after 100 cycles (Z_{Re}

(100^{th} cycle) - Z_{Re} (1^{st} cycle) = $\Delta Z_{Re} \approx 10$ ohm), as compared to the cell with the PE separator ($\Delta Z_{Re} \approx$ 72 ohm).

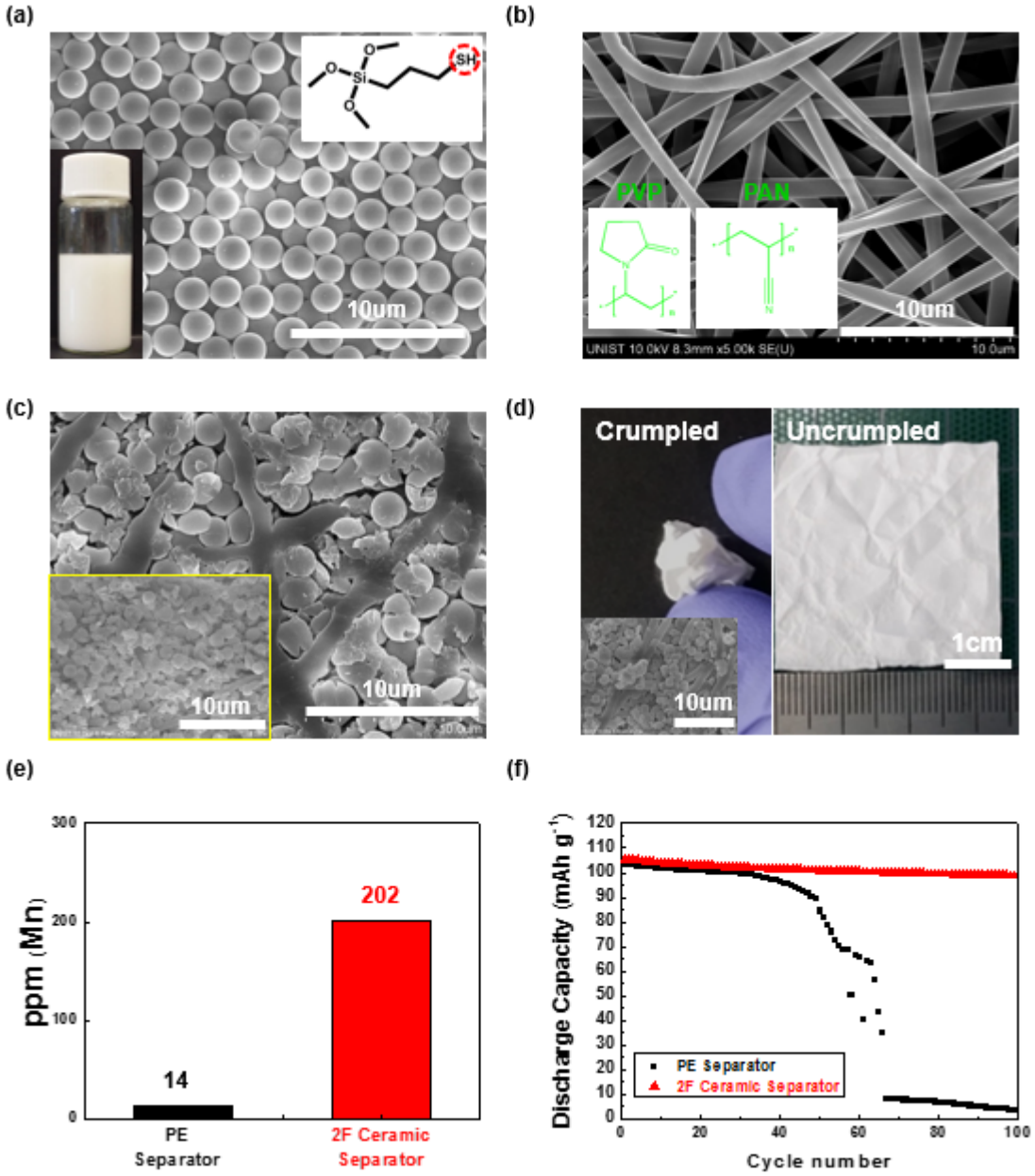

Figure 12. Fabrication and characterization of 2F ceramic separator: (a) a SEM image of F-silica particles (insets show chemical structure of F-silica particles and physical appearance of F-silica particle solution, respectively); (b) a SEM image of electrospun PVP/PAN nanofiber mat (an inset shows chemical structure of PVP and PAN); (c) a SEM image (an inset = cross-sectional view); (d) photographs and a SEM image showing structural tolerance after being subjected to extreme deformation (here, crumpling) test. Comparison between 2F ceramic separator and PE separator; (e) amount of Mn^{2+} ions captured by the separators (estimated from ICP-MS analysis); (f) high-temperature (60 ^{o}C) cycling performance.

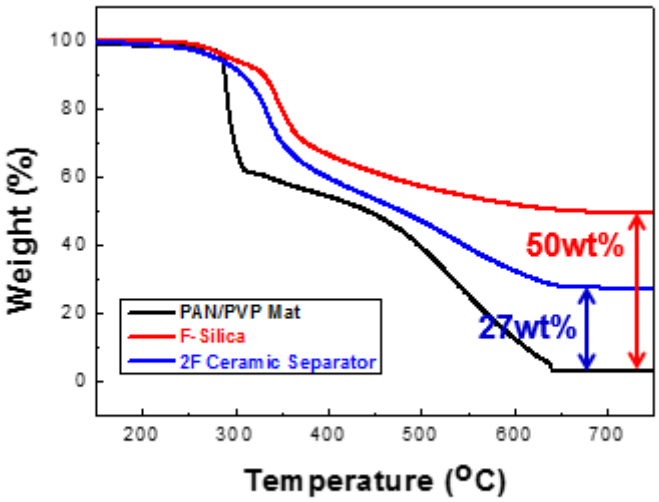

Figure 13. A TGA profile used for estimating the composition ratio of 2F ceramic separator. As a reference sample, TGA profiles of electrospun PVP/PAN nanofiber mat and F-silica were also provided.

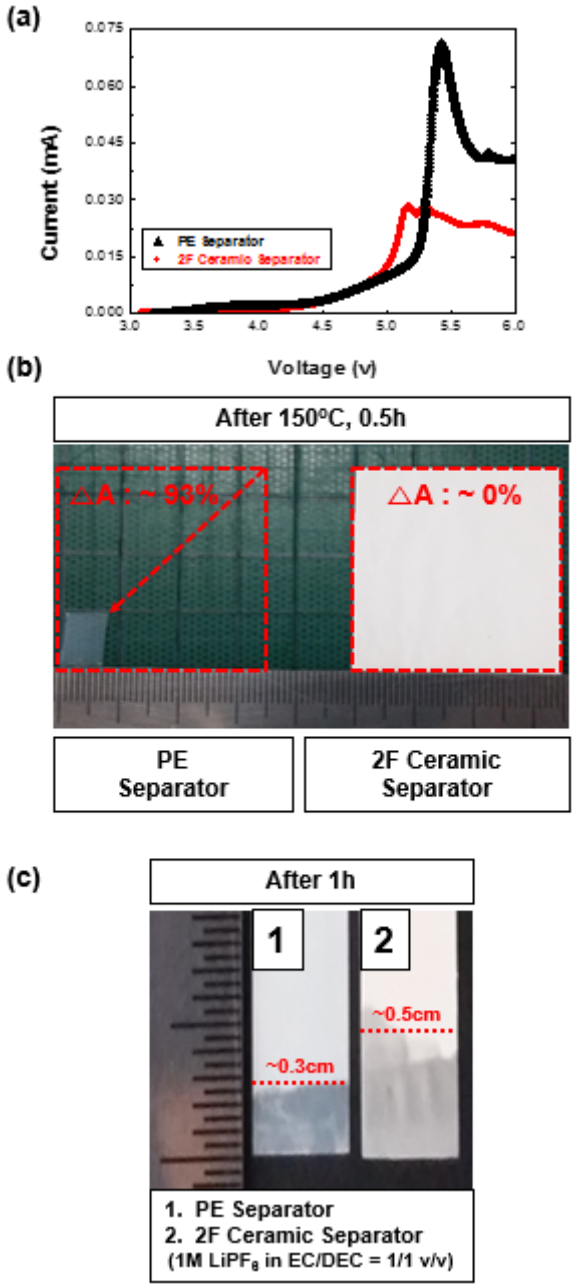

Figure 14. Comparision in basic membrane properties between 2F ceramic separator and PE separator: (a) electrochemical stability window measured by linear sweep voltammetry; (b) thermal shrinkage after exposure to 150 °C/0.5 h; (c) electrolyte wettability (determined by electrolyte-immersion height).

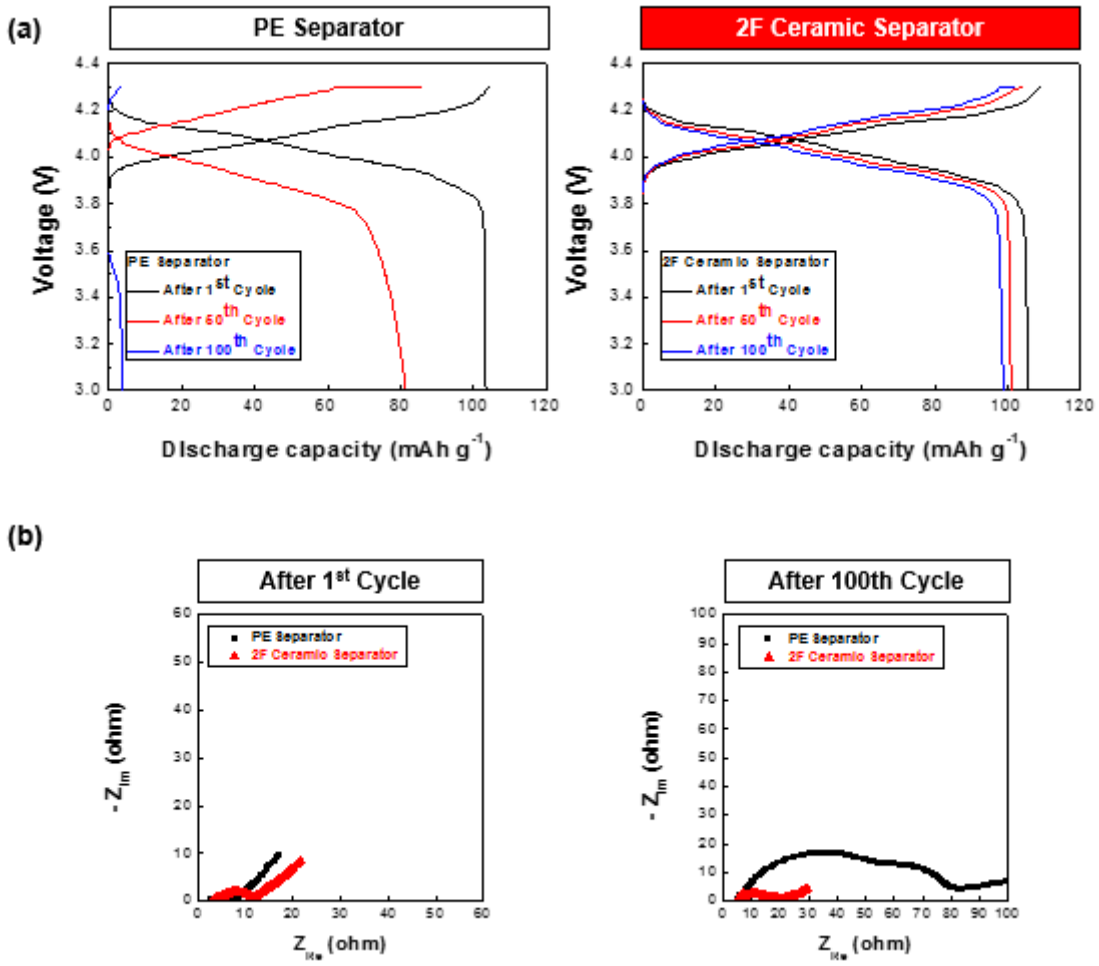

Figure 15. Comparison in cycling performance between 2F ceramic separator and PE separator: (a) charge/discharge profiles as a function of cycle number; (b) change in AC impedance spectra before/after 100 cycles.

2.3.3. The functional influence of 2F ceramic separator: Chelating ability In-depth analysis of 2F ceramic separator

The advantageous effects of the 2F ceramic separator on the cycling performance were elucidated in great detail, with a particular focus on its Mn^{2+}-chelating ability. After the 60 ^{o}C cycling test (100 cycles), the cell was disassembled and then its major components including lithium metal anode, LMO cathode and separator were characterized. The ICP-MS results (Figure 16a) exhibit that the 2F ceramic separator suppresses the deposition of metallic Mn (130 ppm) on the lithium metal, as compared to the PE separator (200 ppm). Moreover, the relatively clean surface was observed at the LMO cathode assembled with the 2F ceramic separator (Figure 16b), while the LMO cathode combined with the PE separator was covered with significant amount of byproducts (an inset of Figure 16b). The byproducts formed on the LMO cathode surface were further characterized using the X-ray photoelectron spectroscopy (XPS) F 1s spectra. For the LMO cathode assembled with the PE separator, a peculiar peak (684.6 eV) assigned to MnF_2 was observed (Figure 16c). The MnF_2 byproducts[36, 37] are known to be generated by side reactions between hydrofluoric acid (HF, produced from residual water-triggered electrolyte decomposition) and dissolved Mn^{2+} ions. By comparison, for the 2F ceramic separator, the LMO cathode shows a peak (687.0 eV) ascribed to a typical SEI layer (including $Li_xPO_yF_z$-containing compounds[38]).

In addition to the abovementioned results of Li metal anode and LMO cathode, the surface change of the 2F ceramic separator with the high-temperature cycling was analyzed. A significant amount of byproducts were formed on the surface of the 2F ceramic separator (Figure 16d), in comparison to that of the PE separator with relatively clean surface (Figure 17). The EDS analysis (focusing on Mn element, Figure 18a) and XPS Mn 2p/F 1s spectra (Figure 18b) exhibit that the byproducts on the 2F ceramic separator surface are attributed to MnF_2-based compounds, verifying that the 2F ceramic separator (as a chemical trap) chelates Mn^{2+} ions during the high-temperature cycling. Such unusual chelating ability of the 2F ceramic separator was further elucidated by monitoring the change in the FT-IR peaks and XPS spectra of the 2F ceramic separator. Figure 16e shows that the characteristic peaks corresponding to thiol (2580 cm^{-1}, F-silica) and C=O/C-N groups (1661 cm^{-1}/1285 cm^{-1}, PVP/PAN nanofiber skeleton) were diminished after the cycling test (100 cycles). Moreover, the intensities of characteristic XPS peak dedicated to S 2p (F-silica) were decreased after 100 cycles (Figure 16f). Both the FT-IR and XPS results clearly demonstrate the 2F ceramic separator-driven chelation of Mn^{2+} ions during the high-temperature (60 ^{o}C) charge/discharge cycling.

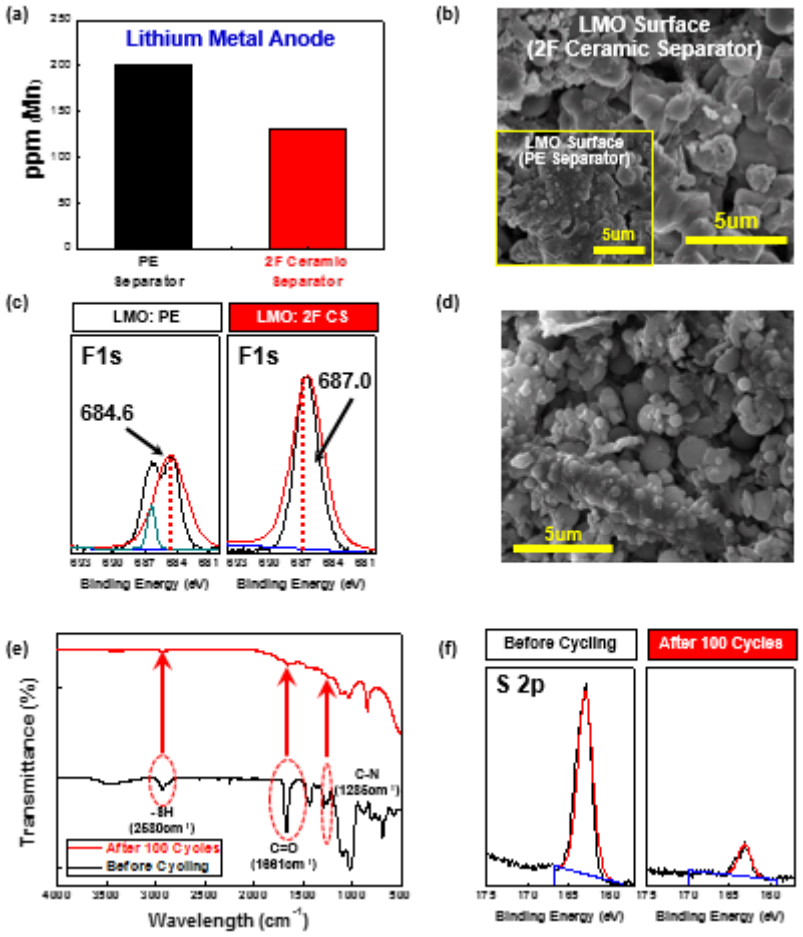

Figure 16. (a)-(c) Structural analysis of LMO cathode and Li metal anode after 100 cycles at 60 °C: (a) metallic Mn deposited on lithium metal anode (from ICP-MS analysis); (b) a SEM image of LMO cathode surface assembled with 2F ceramic separator, wherein an inset shows LMO cathode surface assembled with PE separator; (c) XPS F 1s spectra of LMO surface. (d)-(f) Structural analysis of 2F ceramic separator 100 cycles at 60 °C: (d) a SEM image; (e) FT-IR spectra showing the change in characteristic peaks of thiol (2580 cm^{-1}, F-silica) and C=O/C-N groups (1661 cm^{-1}/1285 cm^{-1}, PAN/PVP nanofiber skeleton); (f) intensity change of XPS S 2p spectra.

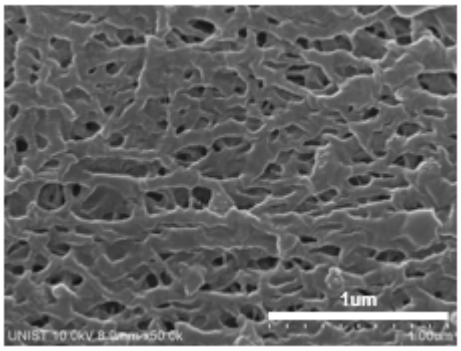

Figure 17. A SEM image of PE separator after 100 cycles at 60 ºC.

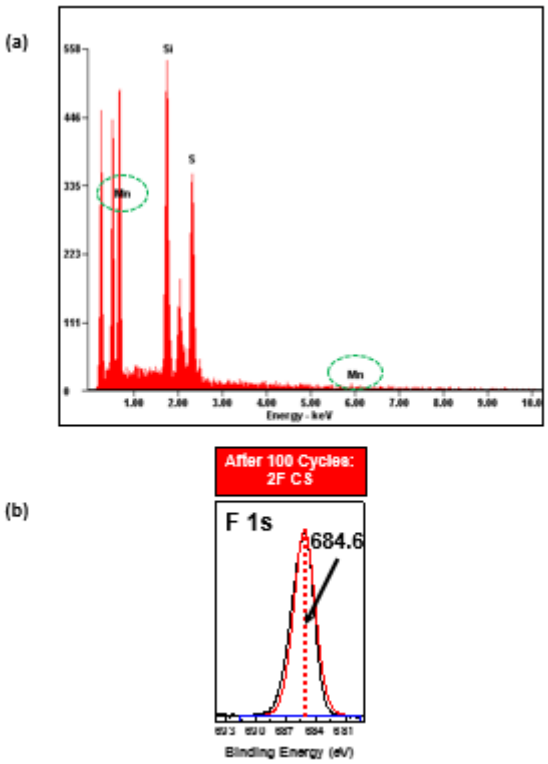

Figure 18. Structural analysis of 2F ceramic separator after 100 cycles at 60 ^{o}C: (a) EDS spectra (focusing on Mn element); (b) XPS F 1s spectra.

The advantageous effect of the 2F ceramic separator on the high-temperature cycling performance is conceptually illustrated in Figure 19. For conventional cells incorporating the commercial PE separator, the Mn^{2+} ions dissolved in liquid electrolyte lead to metallic Mn on the lithium metal anode and also MnF_2-containing resistitve layers on the LMO cathode. By comparison, a considerable amount of Mn^{2+} ions are captured by the 2F ceramic separator (specifically, thiol groups of F-silica particles and pyrrolidone groups of PVP) in the form of Mn(II) chelate complexes, eventually suppressing the Mn^{2+} ions-triggered harmful influence on the electrochemical activity of the electrodes.

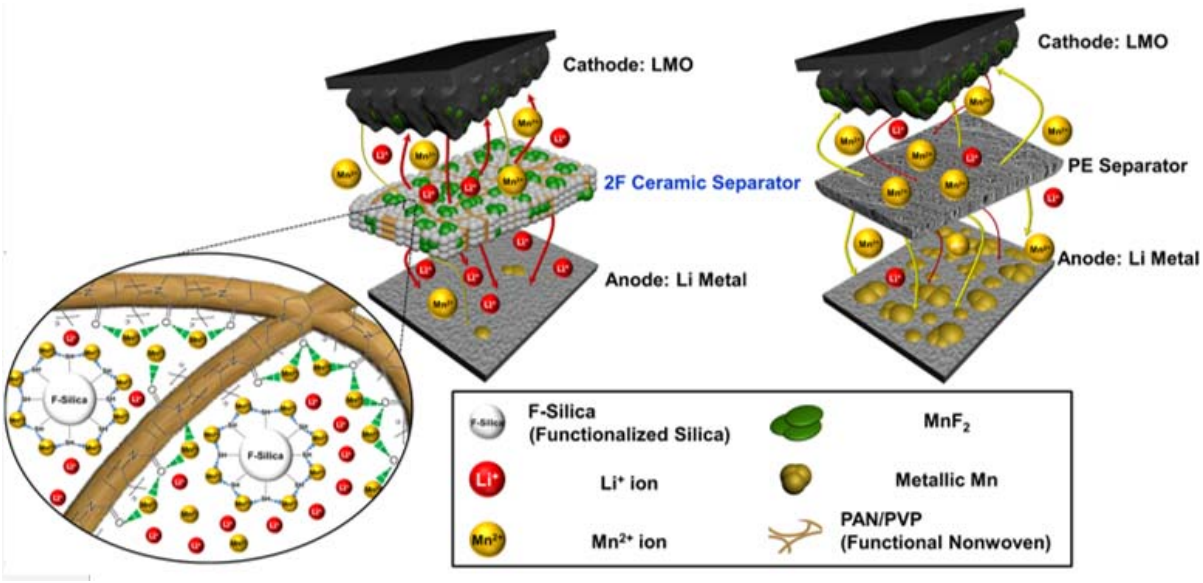

Figure 19. A conceptual illustration depicting advantageous effect of 2F ceramic separator on high-temperature cycling performance. A considerable amount of dissolved Mn^{2+} ions are captured by the 2F ceramic separator in the form of Mn(II) chelate complexes, eventually suppressing the Mn^{2+} ions-triggered negative influence on the electrochemical performance of electrodes.

2.4. Conclusion

In summary, as a ceramic-driven material/architecture strategy to develop an ultimate battery separator far beyond traditional polymeric ones, we have demonstrated the superlattice crystals-mimic 2F ceramic separator with chemical traps for chelating heavy metal ions (here, Mn^{2+}). The 2F ceramic separator, which was comprised of the densely-packed F-silica particles spatially besieged by the PVP/PAN nanofiber skeleton, was fabricated using the simultaneous electrospraying/electrospinning process. The proof of concept for the 2F ceramic separator, from the viewpoint of manufacturing process and basic membrane properties, was explored with a model ceramic separator based on the electrosprayed Al_2O_3 particles and electrospun PVdF nanofibers. The superlattice crystals-mimic structural uniqueness of the close-packed ceramic particles, in combination with the well-designed electrospun nanofiber skeleton, provided remarkable advances in the thermal/dimensional tolerance, mechanical flexibility and other separator properties. Furthermore, both the F-silica particles and PVP/PAN nanofibers possessed the Mn^{2+}-chelating ability, which served as chemical traps for Mn^{2+} ions during their passage through the liquid electrolyte-filled interstitial voids of the 2F ceramic separator. As a consequence, the 2F ceramic separator enabled unprecedented improvements in the high-temperature (60 ^{o}C) cycling performance. Such advantageous effect of the 2F ceramic separator was quantitatively elucidated, with a particular focus on the surface analysis of the electrodes as well as the 2F ceramic separator. Owing to the abovementioned structural uniqueness and chemical functionality, the 2F ceramic separator will hold a great deal of promise as a chemically-active separator for high-performance batteries that are eager to adopt high-energy (but, struggling with metal dissolution) electrode materials and also open a new ceramic opportunity for next-generation multifunctional membranes that are in strong pursuit of selectivity removing heavy metal ions.

Reference

[1] P. Arora, Z. Zhang, *Chem. Rev.* **2004**, *104*, 4419.
[2] H. Lee, M. Yanilmaz, O. Toprakci, K. Fu, X. Zhang, *Energy Environ. Sci.* **2014**, *7*, 3857.
[3] X. Huang, *J. Solid State Electrochem.* **2011**, *15*, 649.
[4] M. Armand, J.-M. Tarascon, *Nature* **2008**, *451*, 652.
[5] B. Scrosati, J. Garche, *J. Power Sources* **2010**, *195*, 2419.
[6] J. Tollefson, *Nature* **2008**, *456*, 436.
[7] B. Dunn, H. Kamath, J.-M. Tarascon, *Science* **2011**, *334*, 928.
[8] V. Etacheri, R. Marom, R. Elazari, G. Salitra, D. Aurbach, *Energy Environ. Sci.* **2011**, *4*, 3243.
[9] J. Hassoun, K. S. Lee, Y. K. Sun, B. Scrosati, *J Am Chem Soc* **2011**, *133*, 3139.
[10] S. S. Zhang, *J. Power Sources* **2007**, *164*, 351.
[11] H.-S. Jeong, D.-W. Kim, Y. U. Jeong, S.-Y. Lee, *J. Power Sources* **2010**, *195*, 6116.
[12] T.-H. Cho, M. Tanaka, H. Ohnishi, Y. Kondo, M. Yoshikazu, T. Nakamura, T. Sakai, *J. Power Sources* **2010**, *195*, 4272.
[13] J. H. Kim, J. H. Kim, K. H. Choi, H. K. Yu, J. H. Kim, J. S. Lee, S. Y. Lee, *Nano Lett.* **2014**, *14*, 4438.
[14] J.-K. Kim, G. Cheruvally, X. Li, J.-H. Ahn, K.-W. Kim, H.-J. Ahn, *J. Power Sources* **2008**, *178*, 815.
[15] J. Coronas, J. Santamaria, *Catal. Today* **1999**, *51*, 377.
[16] A. Julbe, D. Farrusseng, C. Guizard, *J. Membr. Sci.* **2001**, *181*, 3.
[17] K. E. Mueggenburg, X. M. Lin, R. H. Goldsmith, H. M. Jaeger, *Nat Mater* **2007**, *6*, 656.
[18] T. Ding, K. Song, K. Clays, C.-H. Tung, *Adv. Mater.* **2009**, *21*, 1936.
[19] C. Li, L. Qi, *Adv Mater* **2010**, *22*, 1494.
[20] M. S. Whittingham, *Chem. Rev.* **2004**, *104*, 4271.
[21] D. K. Kim, P. Muralidharan, H.-W. Lee, R. Ruffo, Y. Yang, C. K. Chan, H. Peng, R. A. Huggins, Y. Cui, *Nano Lett.* **2008**, *8*, 3948.
[22] M.-H. Ryou, S. Hong, M. Winter, H. Lee, J. W. Choi, *J. Mater. Chem. A* **2013**, *1*, 15224.
[23] M. J. Lee, S. Lee, P. Oh, Y. Kim, J. Cho, *Nano Lett.* **2014**, *14*, 993.
[24] F. Wu, N. Li, Y. Su, L. Zhang, L. Bao, J. Wang, L. Chen, Y. Zheng, L. Dai, J. Peng, S. Chen, *Nano Lett.* **2014**, *14*, 3550.
[25] J. S. Kim, K. Kim, W. Cho, W. H. Shin, R. Kanno, J. W. Choi, *Nano Lett.* **2012**, *12*, 6358.
[26] T. Yim, H.-J. Ha, M.-S. Park, K. J. Kim, J.-S. Yu, Y.-J. Kim, *RSC Adv.* **2013**, *3*, 25657.
[27] S. H. Woo, H. W. Lim, S. Jeon, J. J. Travis, S. M. George, S. H. Lee, Y. N. Jo, J. H. Song, Y. S. Jung, S. Y. Hong, N. S. Choi, K. T. Lee, *J. Electrochem. Soc.* **2013**, *160*, A2234.
[28] A. Jaworek, A. Krupa, M. Lackowski, A. T. Sobczyk, T. Czech, S. Ramakrishna, S. Sundarrajan, D. Pliszka, *J. Electrost.* **2009**, *67*, 435.
[29] M. Yanilmaz, Y. Lu, M. Dirican, K. Fu, X. Zhang, *J. Membr. Sci.* **2014**, *456*, 57.
[30] C. Oh, S.-B. Shim, Y.-G. Lee, S.-G. Oh, *Mater. Res. Bull.* **2011**, *46*, 2064.
[31] S. Wu, F. Li, R. Xu, S. Wei, G. Li, *J. Nanopart. Res.* **2009**, *12*, 2111.
[32] L. Mercier, T. J. Pinnavaia, *Adv. Mater.* **1997**, *9*, 500.
[33] T. Pinnavaia, *Chem. Commun.* **1999**, 69.
[34] X. Feng, G. Fryxell, L.-Q. Wang, A. Y. Kim, J. Liu, K. Kemner, *Science* **1997**, *276*, 923.
[35] J. M. Kim, J. H. Park, C. K. Lee, S. Y. Lee, *Sci Rep* **2014**, *4*, 4602.

[36] S.-T. Myung, K. Izumi, S. Komaba, H. Yashiro, H. J. Bang, Y.-K. Sun, N. Kumagai, *J. Phys. Chem. C* **2007**, *111*, 4061.
[37] F. T. Quinlan, K. Sano, T. Willey, R. Vidu, K. Tasaki, P. Stroeve, *Chem. Mater.* **2001**, *13*, 4207.
[38] K. Edström, T. Gustafsson, J. O. Thomas, *Electrochim. Acta* **2004**, *50*, 397.

Acknowledgement

강원도 토박이로만 살다가, 울산광역시로 이사 와서 연구를 시작한 것이 엊그제 같은데, 벌써 졸업을 앞두고 있다는 점이 감회가 새롭습니다. 어쩌면 저의 인생에 있어, 석사 연구 기간이 없었을 수도 있었을 텐데, 저에게 새롭고, 좋은 도전을 할 수 있는 기회를 가질 수 있도록 도와주시고, 올바르게 지도해 주신 저의 지도 교수님인 이상영 교수님께 먼저 감사의 인사를 드리고 싶습니다. 교수님의 보살핌 덕분에 석사 기간 동안 무탈하게 잘 마칠 수 있었던 것 같습니다. 아직도 많이 부족하고, 모자란 저이지만, 교수님께서 지도해 주신 방법들을 잘 숙지하여, 늘 발전하고, 노력하여 저의 분야에서 잘 할 수 있는 사람이 되도록 하겠습니다.

바쁘신 와중에도 저의 석사 논문 심사에 참석해주신, 박수진 교수님과 김영식 교수님께도 감사의 말씀 전합니다.

저가 이렇게 무사하게 석사 졸업을 할 수 있도록 도와줬던 많은 분들 중에 우선적으로 저의 사수였던 은선이 형에게 감사의 말을 전하고 싶습니다. 저도 사수가 되보고 직접 경험해보니까, 형이 저 때문에 느꼈을 스트레스가 참 많았을 것 같다는 생각이 듭니다. 실험실에서 나갈 때까지, 나가서까지도 많이 도와주시고, 챙겨주셔서 너무 너무 감사합니다. 형 덕분에 많은 것들을 배울 수 있었고, 알 수 있었던 것 같습니다. 또한, 학사 동기여서 많이 의지가 되었던, 은혜, 주현, 지혜도 정말 많이 고마워. 힘들고 지칠 때마다 대학원 선배로서, 너희들이 해줬던 말들이 내게는 큰 힘들이 되었던 것 같아. 항상 건강하고, 늘 좋은 일들만 가득하길 바랄게.

장훈이 형, 은호 형, 현석이 형, 종헌이 형, 정란이 누나, 효정이 누나, 낯가림이 심한 저인데, 만날 때 마다 잘 챙겨주시고, 많이 많이 웃게 해주셔서 감사합니다.

준묵이 형과 현지, 근호, 실험실 선배들 떠나고, 실험실 관리하고 챙기느냐고 고생 많이 하셨습니다. 근호는 지금도 충분히 잘하고 있으니까, 좋은 성과 더 많이 많이 내서, 최교수가 되길 바랄게, 준묵이 형 취업에 대해 아무것도 몰랐는데, 덕분에 유용한

정보들도 많이 알 수 있었고, 형 덕분에 실험실 생활이나, 다른 생활부분에 있어서 많은 점들을 배울 수 있었던 것 같아요. 취업 잘되어서 정말 축하 드려요. 누나한테 잘해서, 얼른 국수 먹여주세요! 현지랑은 때로는 선배이자, 동료이자 그랬던 것 같네. 그만큼 힘들 때마다 옆에서 응원해주고 도와줘서 너무 너무 고마워. 덕분에 여기까지 올 수 있지 않았나 싶네. 취업 때문에 스트레스 많이 받았던 걸로 알고 있었는데 잘되어서 너무 너무 축하하고, 가서도 충분히 잘 할거라고 믿어, 가서 좋은 성과 많이 내길 바랄게.

너무 너무 감사하고, 든든한 나의 동기들, 주명, 세희, 성주, 정환

어쩌면 중간에 포기했을 지도 모르고, 강원대에서 졸업을 했을지도 모르지만, 너희들 덕분에 내가 지금 이 자리에 있을 수 있는 것 같아. 그래서 너무 너무 감사하고, 고마워. 정환이는 울산 와서 같이 분리막 맡으면서, 서로 힘들 때마다 기댈 수 있었던 것 같아. 이제는 분리막의 수장이자, 실험실 실장이니까, 지금처럼 책임감 가지고 열심히 하면, 더 좋은 성과 있을 것이라 믿어. 엄격한 관리자인 주명이, 늘 체계적으로 계획새우고, 맡은 일에 대해 철두철미하게 해나가는 주명이 보면서, 직/간접적으로 보고 배운 점이 많은 것 같아. 쉽지 않은 자리에서 포기하지 않고 열심히 노력하는 모습이 정말 멋진 것 같고, 배울 점이 많은 것 같아. 같이 지내오면서, 연구 방식이나 자기 일에 대한 접근 방식이나 처리 방법에 대해 가장 많이 보고 배웠던 것 같아. 그래서 덕분에 좋은 결과를 가지고 석사 과정을 마칠 수 있지 않나 싶고, 그래서 많이 고마워. 지금처럼 만하면, 좋은 결과들은 당연히 따라오지 않을까 싶고, 늘 좋은 일들만 있길 바랄게. 어쩌면 나랑 성격이 가장 비슷한 세희, 그 점 때문에 공감하는 것도 많고, 서로 답답했던 점도 많았던 것 같아. 그래도 서로 힘든 부분들 있으면 의지하고, 도와주고, 위로해 줄 수 있었던 것 같아. 지금도 충분히 잘 하고 있으니까, 자존감/자신감 잘 챙기기 만하면, 충분히 좋은 성과 있을 거라 생각해. 마지막으로 성주, 성주랑은 울산 와서 더욱 친해 진 것 같아. 은근히 많이 챙겨주고, 도와줘서 고마워. 계속 박사 같이 가자고 해줘서 고맙고, 끝까지 함께 하지 못해서 많이 아쉽다. 아직 남아 있는 기간 동안 같이 즐겁게 보냈으면 좋겠고,

성주도 좋은 결과들 많이 많이 나오길 바랄게. 다시 한번 더 우리 동기들 너무 너무 고맙고, 너희와는 다른 길을 선택해서, 마지막까지는 함께하지 못하겠지만, 좋은 결과, 성과들 많이 있고, 늘 건강하길 바랄게.

이박사님/유박사님, 박사님들 덕분에 석사 연구 활동하는데 도움이 많이 되었던 것 같고, 생각하는 힘을 기를 수 있었던 것 같습니다. 유박사님, 연구 할 때는 박사님처럼, 평소에는 형처럼 많이 챙겨주고, 어려운 일 있을 때, 서슴없이 도와주셔서, 감사합니다. 함께 있었던 시간이 짧지만, 임팩트 있었던 시간들 이였던 것 같습니다.

헤이 브라더 창훈, 나에게는 우리 동기들 빼고, 의지 할 수 있었던 사람이었던 것 같아. 자전거타면서 같이 공감했던 부분들도 있고, 이런 저런 부분들에 있어서 의지 할 수 있었던 것 같아서 고마워. 앞으로 좋은 일들만 있기를 바랄게. 정말 쓰고 싶은 말이 있는데 잔소리 될 것 같아서 참을게. 성선/연수/동규/현우/예리, 지금이 가장 힘든 시기지 않을까 싶다. 나도 그랬고, 정신 없이 시간은 가고 불안하고, 잘 모르겠고, 근데 내가 생활해 보니까, 석사 기간이 그렇게 길지만은 않은 것 같아, 그러니까 정신 똑바로 붙잡고, 선배들한테 달라붙어서 얼른얼른 배워서 잘 헤쳐나가길 바랄게. 너희들은 충분히 잘 할거라 믿고, 각자의 위치에서 선/후배들한테도 잘 했으면 좋겠다.

지현/석규/용혁/수정/정아 우리 귀요미 학부생들 이제 너희들은 고생길이 열렸다. 각오 단단히 하고 대학원 들어오고, 지금하고 있는 것처럼 열심히 하면, 석사 또는 석/박사 기간 동안 충분히 좋은 결과들 있을 거라 생각한다. 그리고 맡은 바 일에 대해, 책임을 가지고 잘하는 나의 부사수 지현이, 지금도 충분히 잘하고 있으니까, 너무 급하게 생각하지 말고, 조금은 천천히 완급 조절해가면서, 해나가면 충분히 좋은 결과 있을 것이라 믿는다. 앞으로도 수고하고, 지금처럼 분리막 선배들 일들 잘 도와줬으면 좋겠다.

마지막으로, 윤교형, 태수형, 형들 덕분에, 석사 연구 기간 동안 더 즐겁게 할 수 있지 않았나 싶네요. 태수형은 우리오피스 와서 애들 좀 그만 괴롭히고, 애들 맛있는 것 좀

사주세요. 윤교형은 고마운 점이 너무 너무 많네요. 여기 나가서도 연락하면서 지냈으면 좋겠습니다. 두 형님들도 늘 좋은 일들과 성과들 있기를 바랄게요.

끝으로 사랑하는 우리가족들, 존경하는 우리 아바이, 사랑스러운 우리 어무이, 늘 고마운 우리누나, 늘 믿어주고, 사랑해주고, 전폭적으로 지원해줘서 감사하고, 고맙습니다. 더욱더 발전할 수 있도록 노력하겠습니다. 사랑합니다.